(Preprint) AAS 19-802

OPTIMIZATION OF LOW THRUST TRANSFER ORBITS OF A SPACECRAFT CONSIDERING THE RADIATION HAZARD FROM THE VAN ALLEN BELTS

Rodrigo N. Schmitt[*], Gerson Barbosa[†], Alexander Sukhanov[‡] and Antonio F. B. A. Prado[§]

The goal of this work is to measure the amount of radiation a spacecraft receives once it leaves the sphere of influence of Earth in a Low Thrust Orbit (LTO). The spacecraft crosses the Van Allen belts many times during the transfer, in which particles such as protons and electrons can damage the onboard electronic equipment. Through mathematically modeling of the density of particles from the belt in space, it was possible to integrate it in time and compute the total dose of radiation absorbed by the spacecraft according to the chosen trajectory. Therefore, different trajectories were computed varying in eccentricity and type of propulsion system, which gave the following final parameters of interest: mission duration, fuel consumption, time in Van Allen belts and total fluence of radiation absorbed. Using an optimization algorithm, thousands of trajectories were tested and the best ones with respect to the final parameters were given in a table with the results.

INTRODUCTION

The context of the problem studied is the transfer orbit of a spacecraft from a Low Earth Orbit (LEO) to outside Earth's Sphere of Influence using Solar Electric Propulsion (SEP), thus a low thrust system. The specific impulse of this type of propulsion system is five to ten times greater than the one from ordinary chemical propulsion, which translates to higher efficiency. The following optimization problem can then be considered: finding positions and thrust arcs that maximize the final mass of the spacecraft for a given transfer orbit. However, the spacecraft must cross the Van Allen belts dozens of times during its trajectory due to its low thrust character, which poses a hazard to its electronic equipment due to the radiation exposure. It is then of interest of the mission analyst to optimize the final mass of the vehicle choosing the trajectory that satisfies the radiation limitations, as well as minimizes the fuel consumption and transfer time.

The dynamical system is constituted by a spacecraft that starts its motion in orbit around the Earth - after being detached from the rocket - with fixed orbital elements. After that, the spacecraft is powered by a low thrust propulsion system until it reaches the energy level zero, which means that it achieved a parabolic orbit. The engines operate in an "on-off" mode, such that it uses the greatest

[*]Student, Department of Astronomy, Institute of Astronomy, Geophysics and Atmospheric Sciences of University of Sao Paulo, USP - Butanta, Sao Paulo - SP, 03178-200, Brazil.

[†]Student, National Institute for Space Research, INPE - Av dos Astronautas 1758, Sao Jose dos Campos, Sao Paulo, 12227-010, Brazil.

[‡]Russian National Institute for Space Research, IKI - Moscow, Russia.

[§]President of the Board of the Graduate School, INPE - Av dos Astronautas 1758, Sao Jose dos Campos, Sao Paulo, 12227-010, Brazil.

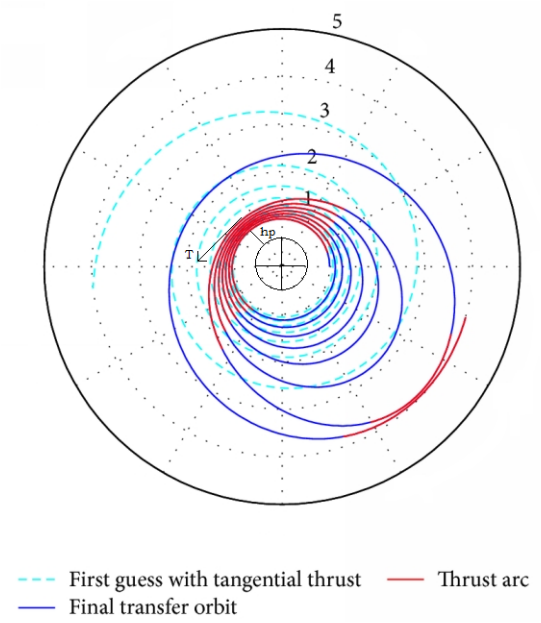

Figure 1. Trajectory of the spacecraft escaping from the Earth.[1]

velocity region near the perigee of the orbit to accelerate the spacecraft. When the spacecraft gets closer to the region near the apogee, the engine is turned off, as illustrated in Figure 1. After a certain number of revolutions, the spacecraft reaches the escape velocity, and its orbit around the Earth becomes parabolic. In this phase, the problem is considered as a "two-body" problem Earth-spacecraft with the addition of the Low Thrust. A family of transfer orbits is built using the total transfer time as a parameter. It means that, based on this value, optimization techniques are used to decide the number and duration of the thrust arcs.

During the transfer, the time the spacecraft spends inside the radiation belts is calculated for each region it is divided, as well as the respective proton and electron integral omnidirectional fluxes absorbed by the spacecraft inside that region. This type of flux takes into account particles coming from all directions with an energy greater than the threshold energy chosen. It is then possible to know the fuel consumed, the total transfer time, the time the spacecraft spends inside the belt and the total radiation it absorbs during the trajectory. This information is enough to build plots that show the options available for a mission designer.

THE OPTIMIZATION METHOD

In order to optimize the thousands of transfer trajectories calculated, the following expression was used to determine the length of each thrust arc:

$$E = F(1 - ce^p) \tag{1}$$

where E is eccentric anomaly of the current thrust arc (i.e. the thrust arc is between -E and E, with $0° < E < 180°$), F is an angular parameter varied between 10 and 180 degrees (corresponding

to the longest and shortest transfer time, respectively), e is eccentricity of the orbit being analyzed, c and p are parameters varied within the limits 1 ¡ c ¡ 1 and 0 ¡ p ¡ 2. The parameter values corresponding to the maximal final spacecraft mass for the given transfer time are selected.

Expression 1 was derived based on the analysis of optimal thrust arcs. An analysis of thousands transfer trajectories with various initial data has shown the final spacecraft mass is very close to one corresponding to the optimal thrust arcs.

EARTH'S MAGNETIC FIELD

The geomagnetic field B is a result of three distinct components: the nuclear field, the crust field and the external field. The nuclear field comes from the convective movement of conductive fluids from the terrestrial nucleus, while the crust field comes from superficial anomalies associated to ferromagnetic materials from the Earth's crust, which suffers geological and tectonic movements. The nuclear and crust fields make up more than 99% of the field B in LEO. However, the external field Be is derived mainly from extraterrestrial sources, like the solar wind, which varies quickly with the solar cycle of about 11 years and is intrinsically related to the geomagnetic activity and solar interactions. Models of the external component exist, but are of limited importance to our models of the Van Allen belts.[2]

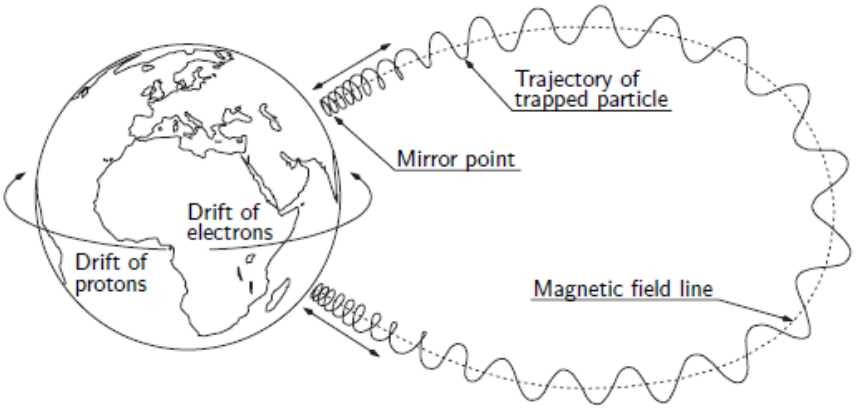

Figure 2. Movement of charged particles due to the interaction with the Earth's magnetic field.[3]

The internal geomagnetic field can be modelled roughly by a magnetic dipole inclined in -11 degrees with respect to the geographic north, with magnitude $M = 8 \times 10^{25} G.cm^2$. The field generated by M in spherical coordinates (r, θ, ϕ) is given by:

$$B_i = -(M/r^2)\sqrt{3cos\theta + 1} \tag{2}$$

This approximation is refined using the expansion in spherical harmonics of the scalar magnetic potential. Bi, then, has a maximum of 0.6 G in the polar region and a minimum of 0.3 G near the magnetic equator.[4]

A charged particle suffers the influence of this magnetic field and will follow a helical trajectory, also known as cyclotron, as illustrated by Figure 2.

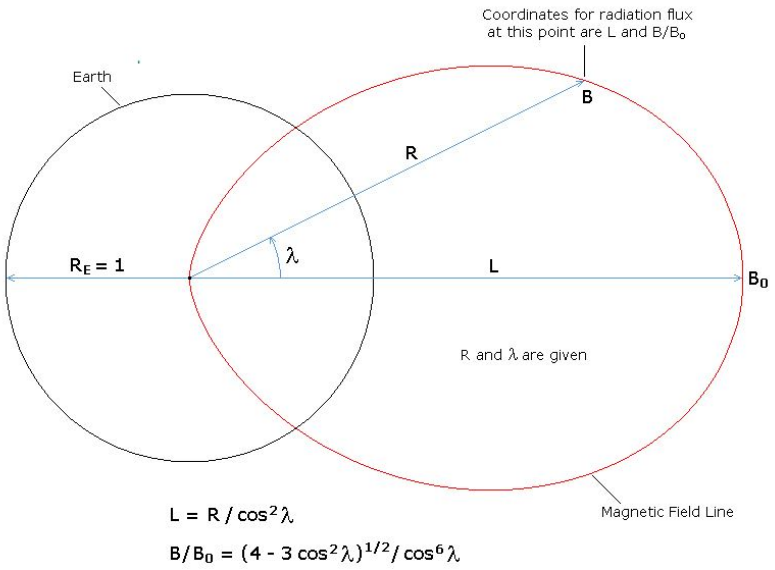

Figure 3. Coordinates for a point in space, given by B and L or R and λ.

Through the conservation of some physical parameters, such as the linear momentum of the particle, it is possible to use two variables to describe the geomagnetic field: the system B-L, in which a population of particles is described in terms of the flux of particles as a function of the values of B and L. The dimensionless quantity L is defined by:

$$L = \frac{r_0}{R_e} \tag{3}$$

where r_0 is the radial distance in which the field line crosses the magnetic equator, and R_e is the Earth's equatorial radius, 6378 km. Therefore, the value of L indicates the point in which the field line of interest crosses the magnetic equator, measured in Earth radius, as illustrated by Figure 3.

The magnitude B of the geomagnetic field, on the other hand, can be calculated as a function of the norm of the magnetic field in the equator, $B_0 = M/L$, and the magnetic latitude, λ:

$$\frac{B}{B_0} = \frac{\sqrt{4 - 3cos^2\lambda}}{cos^6\lambda} \tag{4}$$

Thus, the map the flux of particles in space can be constructed as a function of two coordinates, B and L, which are calculated from the spacial coordinates R and λ.

MODEL OF THE VAN ALLEN BELTS

The computation of the radiation fluxes involves using a model of the Van Allen belts, which was done in the present work by dividing them into a inner belt composed only by protons and an outer belt composed only by electrons. Both belts were modelled by dividing them into a series of regions with fixed proton/electron fluxes, analogous to the ones illustrated in Figure 4. The next step was to calculate the radiation fluxes absorbed by the spacecraft, by computing the total time it spends

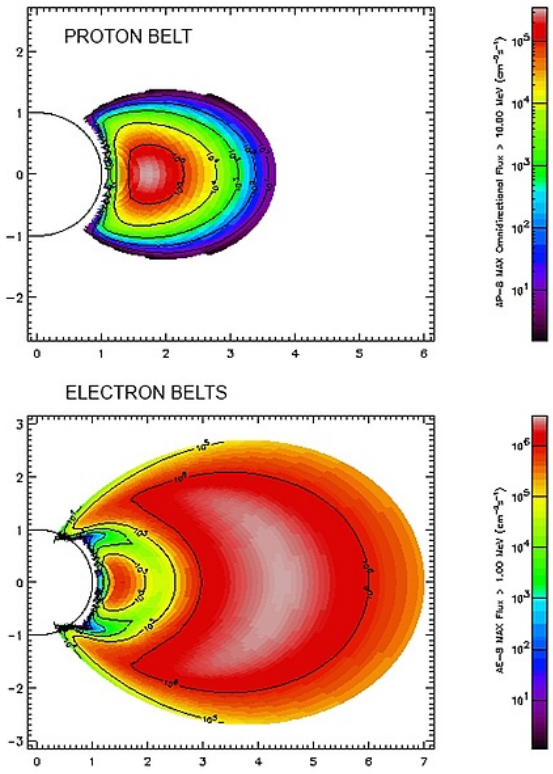

Figure 4. Example of model for the Van Allen Belts; axes x and y are measured in Earth radius, 6378 km.[5]

in each region of the proton, as well as the electron belt. Finally, the radiation resulting fluence is obtained.

Figure 4 presents the model from Spenvis,[5] in which data from space missions (AP8 and AE8) are used to spatially model the omnidirectional integral flux of protons and electrons. The threshold energy used in this model is 10 MeV for protons and 1 MeV for electrons.

An analogous model was developed in Matlab through an algorithm in C made by NASA,[6] which used data from space missions to calculate the omnidirectional integral flux in each point of space, with a chosen threshold energy. The algorithm was optimized and provided the values of the proton flux, electron flux, B/B_0 and L for a given point inside the Van Allen Belts with polar coordinates R (distance to the center of the Earth) and λ, the magnetic latitude. The threshold energy chosen was 0.15 MeV for electrons and 4.0 MeV for protons, more permissive values that allow a more conservative analysis.

Figure 5 presents the contour map made for the proton belt, in which the omnidirectional integral fluxes of protons are mapped, in particles/$(cm^2.s)$, for each point in space. Figure 6 presents the contour map made for the electron belt, in which the omnidirectional integral fluxes of protons are mapped, in particles/$(cm^2.s)$, for each point in space.

Using the results above, the radiation belt models were used in the optimization of the trajectory to obtain the fluences of protons and electrons as a function of mission time. These programs were

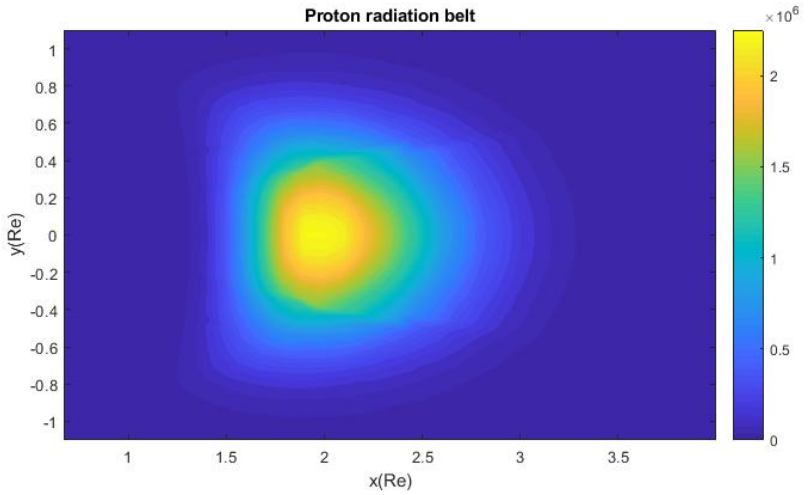

Figure 5. Contour map of the omnidirectional integral flux of protons; Re = 6378 km

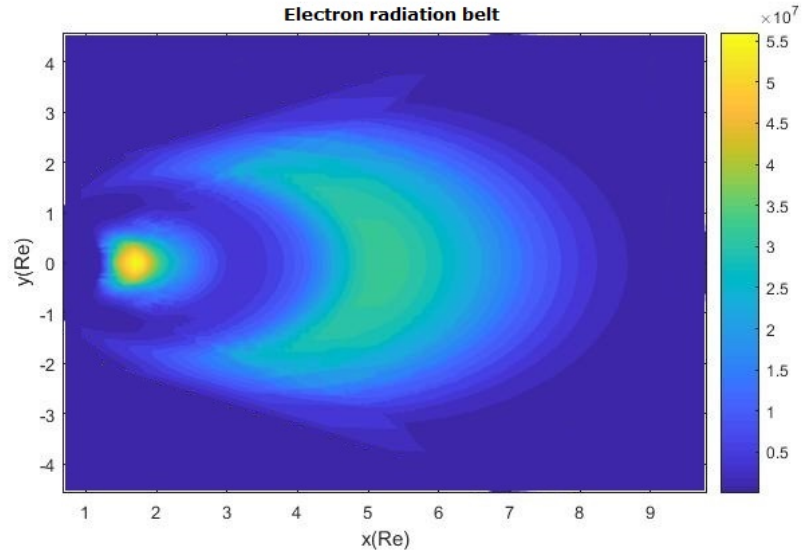

Figure 6. Contour map of the omnidirectional integral flux of electrons; Re = 6378 km

included as part of a more extensive code for orbit determination and optimization developed by Sukhanov et. al.[7]

RESULTS

The code ran 12 times with the same initial spacecraft mass ($m = 160kg$) and the same final energy ($\epsilon = 0$, which indicates the spacecraft leaves earth in a parabolic trajectory). The following initial conditions were chosen: the thrust T and specific impulse I_{sp} of the propulsion system; the perigee altitude h_p and the eccentricity e of the initial orbit. Two propulsion systems were chosen,

the first with $T = 72mN$ and $I_{sp} = 2700s$, which will be called Propulsion System A, and the second with $T = 94mN$ and $I_{sp} = 2300s$, which will be called Propulsion System B. Furthermore, two values for altitude of perigee were chosen, namely $h_p = 600km$ e $h_p = 1200km$, and three initial eccentricities were chosen: $e = 0$, $e = 0.4$ and $e = 0.8$.

The final parameters are as follows: total number of orbits; total time of the mission, in months; final mass of the spacecraft, in kg; fluence of protons once the trajectory is complete, in particles/cm^2; fluence of electrons once the trajectory is complete, in particles/cm^2; total fluence of particles once the trajectory is complete, in particles/cm^2; and time inside the electron belt, in days. This last one represents the time inside the Van Allen belts, since the model for the electron belt extends to the end of the Van Allen belts, contrary to the proton belt.

The plots from Figures 7, 8, 9 and 10 present the most important results obtained - final mass, time inside the electron belt, fluence of protons and fluence of electrons, respectively - as functions of mission time, for the three initial eccentricities chosen (0, 0.4 and 0.8).

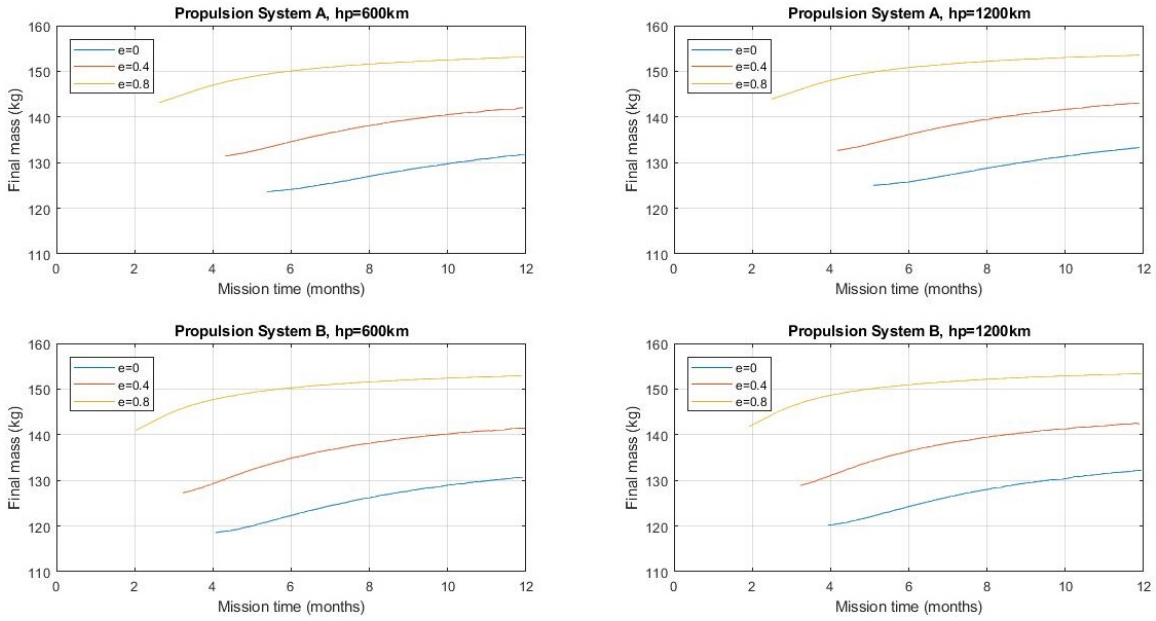

Figure 7. Final spacecraft mass as a function of mission time for each Propulsion System and initial height.

It is evident through Figures 7, 8, 9 and 10 that the behaviour of Propulsion System A is very similar to the one from Propulsion System B, both with respect to final mass, time inside the belts and fluence of particles. However, Propulsion System B allows a faster passage through the belts, since the plots of "Time in the belts x Mission Time" are slightly lower in this case. The plots of proton fluence also show a slightly lower exposure to this type of particle when using Propulsion System B. The plots of fluence of electrons, on the other hand, don't change significantly with the choice of propulsion type.

An immediate analysis is the resemblance between the relationships of "Fluence x Mission Time" and "Time in the belts x Mission Time": as expected, the fluence of particles behaves in a similar fashion as the time inside the belts, since it comes from it. Both follow an almost linear relationship with the time of the mission, for all eccentricities. An interesting aspect, however, is the gap between

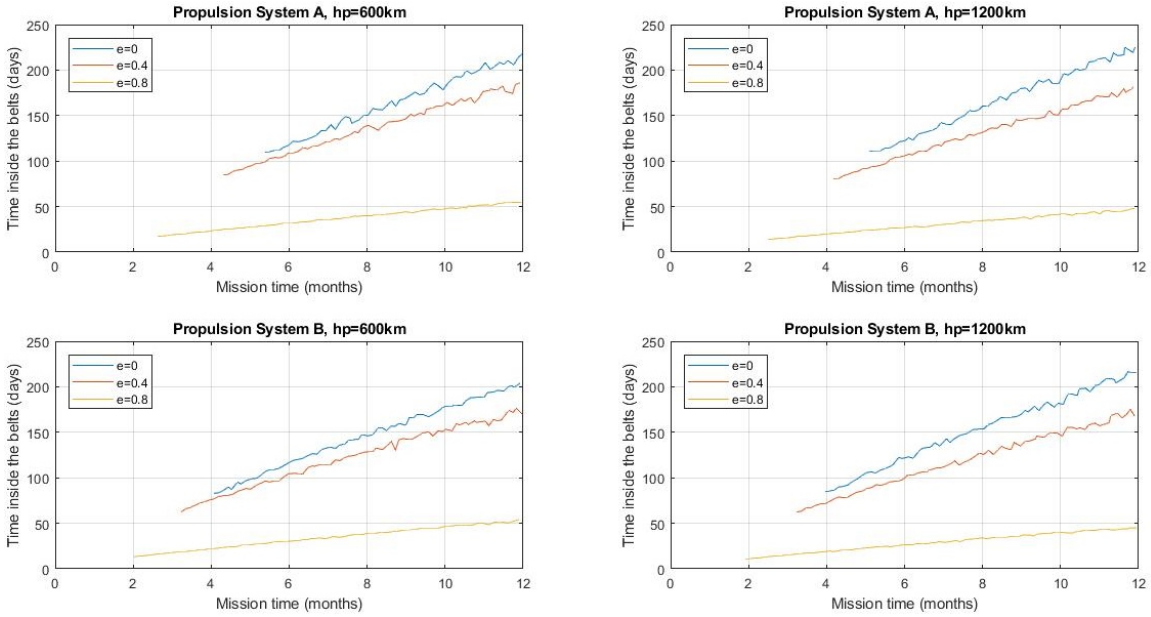

Figure 8. Time inside the belts as a function of mission time for each Propulsion System and initial height.

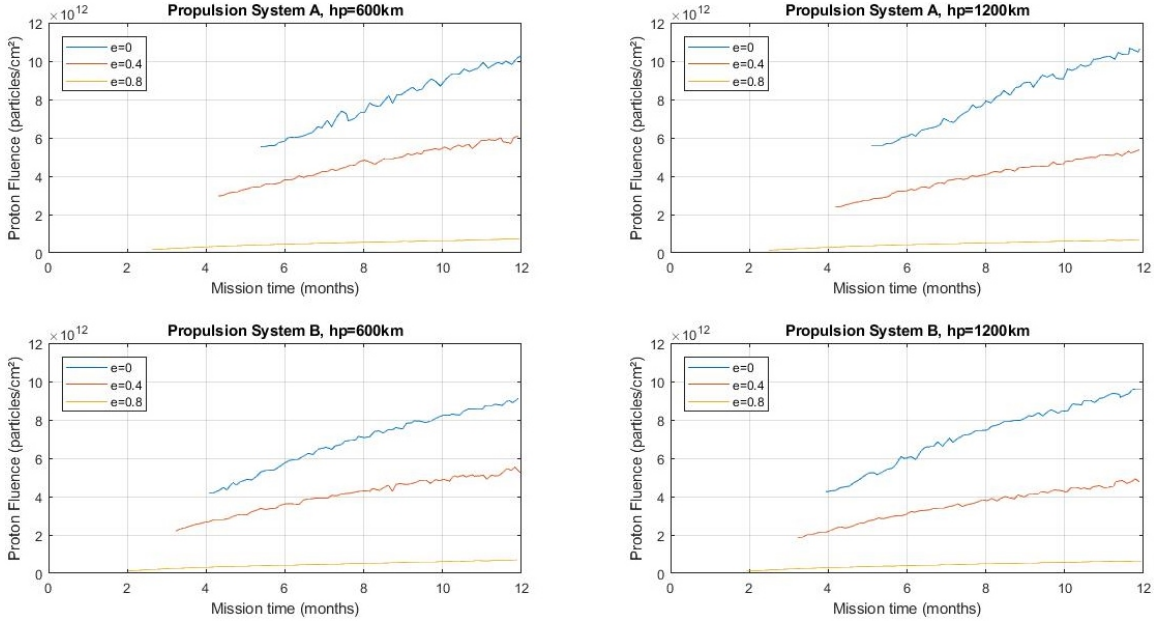

Figure 9. Fluence of protons as a function of mission time for each Propulsion System and initial height.

eccentricities 0.4 and 0.8: the time inside the belts doesn't vary much between the curves, while the fluence of radiation has a wider interval, for both propulsion systems. That justifies the analysis of absorbed radiation, since it gives us richer data than the time inside the belts.

We can also draw conclusions with respect to the eccentricity: as it rises, the greater the final

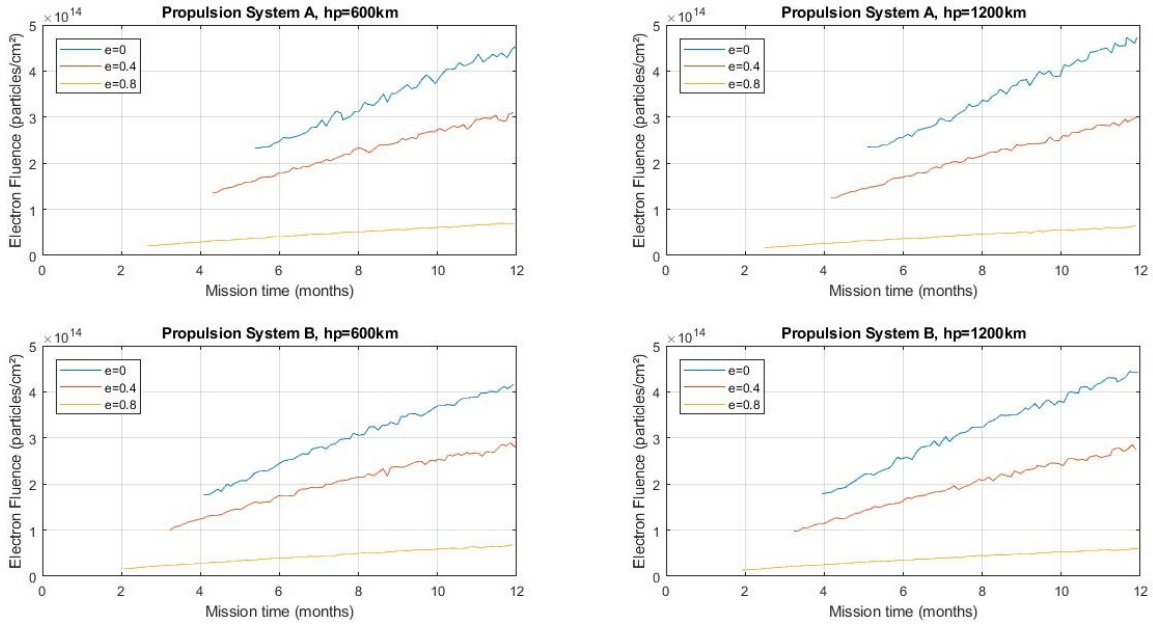

Figure 10. Fluence of electrons as a function of mission time for each Propulsion System and initial height.

mass, the lower the time inside the belts and the lower the radiation fluences. Therefore, we can conclude that higher eccentricities are beneficial to all analyzed parameters, minimizing fuel consumption as well as the exposure to radiation.

One final comparative analysis can be made with respect to the initial height: it doesn't affect deeply the final parameters for the chosen values. Since 600 km and 1200 km didn't result in significant differences, the height can be chosen as the former, as it is more economic to put the spacecraft into a lower orbit.

Table 1 presents one of the 12 results of the algorithm for trajectory optimization. The initial conditions for this result are the following: hp = 600km, e = 0 and Propulsion Type A.

Table 1: Results for: Propulsion System A, hp = 600km, e = 0

Mission Time (months)	Final Mass (kg)	Total Fluence $(1/cm^2)$	Proton Fluence $(1/cm^2)$	Electron Fluence $(1/cm^2)$	Time inside belts (days)
5.273	123.56	2.33E+14	5.54E+12	2.27E+14	109.87
5.396	123.65	2.33E+14	5.54E+12	2.27E+14	109.77
5.502	123.73	2.33E+14	5.55E+12	2.28E+14	110.26
5.608	123.81	2.36E+14	5.60E+12	2.30E+14	111.54
5.743	123.9	2.36E+14	5.60E+12	2.30E+14	111.51
5.838	123.98	2.42E+14	5.74E+12	2.36E+14	114.67
5.992	124.15	2.47E+14	5.84E+12	2.41E+14	117.51
6.102	124.22	2.56E+14	6.04E+12	2.50E+14	121.75
6.236	124.38	2.54E+14	6.01E+12	2.48E+14	121.07

Table 1 - continued

6.33	124.55	2.56E+14	6.03E+12	2.50E+14	122.31
6.441	124.7	2.58E+14	6.08E+12	2.52E+14	123.54
6.563	124.85	2.63E+14	6.18E+12	2.56E+14	125.59
6.694	125.06	2.67E+14	6.28E+12	2.61E+14	128.13
6.829	125.22	2.79E+14	6.57E+12	2.73E+14	133.56
6.934	125.4	2.78E+14	6.52E+12	2.71E+14	133.18
7.073	125.54	2.93E+14	6.91E+12	2.86E+14	140.01
7.184	125.7	2.81E+14	6.58E+12	2.74E+14	134.61
7.314	125.92	3.01E+14	7.08E+12	2.93E+14	143.48
7.436	126.01	3.13E+14	7.40E+12	3.06E+14	148.78
7.558	126.32	3.09E+14	7.26E+12	3.01E+14	147.38
7.606	126.38	2.94E+14	6.87E+12	2.87E+14	141.53
7.78	126.65	3.01E+14	7.03E+12	2.94E+14	144.87
7.909	126.86	3.13E+14	7.33E+12	3.05E+14	149.79
8.023	127.04	3.13E+14	7.33E+12	3.06E+14	150.34
8.149	127.2	3.32E+14	7.81E+12	3.24E+14	157.89
8.24	127.38	3.28E+14	7.70E+12	3.20E+14	156.78
8.392	127.59	3.25E+14	7.62E+12	3.18E+14	156.33
8.484	127.73	3.34E+14	7.83E+12	3.26E+14	159.75
8.631	127.92	3.50E+14	8.21E+12	3.41E+14	166.31
8.73	128.05	3.33E+14	7.79E+12	3.25E+14	159.99
8.838	128.23	3.51E+14	8.23E+12	3.43E+14	167.21
8.942	128.4	3.52E+14	8.24E+12	3.43E+14	167.87
9.101	128.61	3.62E+14	8.46E+12	3.53E+14	172.07
9.233	128.78	3.70E+14	8.64E+12	3.61E+14	175.78
9.341	128.93	3.62E+14	8.46E+12	3.53E+14	172.79
9.474	129.1	3.65E+14	8.54E+12	3.56E+14	174.3
9.591	129.23	3.80E+14	8.85E+12	3.72E+14	180.66
9.718	129.36	3.92E+14	9.07E+12	3.83E+14	185.75
9.825	129.54	3.84E+14	8.93E+12	3.75E+14	182.74
9.943	129.63	3.73E+14	8.70E+12	3.64E+14	178.28
10.079	129.87	3.90E+14	9.05E+12	3.81E+14	185.87
10.191	130	4.01E+14	9.26E+12	3.92E+14	190.83
10.271	130.09	4.05E+14	9.35E+12	3.96E+14	192.78
10.427	130.26	4.04E+14	9.33E+12	3.94E+14	192.17
10.542	130.32	4.18E+14	9.59E+12	4.09E+14	199.14
10.677	130.51	4.11E+14	9.46E+12	4.02E+14	195.92
10.731	130.63	4.13E+14	9.50E+12	4.03E+14	196.72
10.892	130.81	4.19E+14	9.63E+12	4.10E+14	200.26
11.028	130.84	4.36E+14	9.93E+12	4.26E+14	208.13
11.159	131.06	4.19E+14	9.64E+12	4.10E+14	200.61
11.258	131.14	4.26E+14	9.76E+12	4.17E+14	203.57
11.397	131.32	4.36E+14	9.94E+12	4.26E+14	208.35
11.507	131.42	4.30E+14	9.84E+12	4.21E+14	206.13
11.604	131.44	4.40E+14	1.00E+13	4.30E+14	210.37

Table 1 - continued

11.758	131.59	4.29E+14	9.83E+12	4.19E+14	205.77
11.878	131.77	4.47E+14	1.01E+13	4.37E+14	214.04
11.993	131.84	4.55E+14	1.03E+13	4.44E+14	218.11

CONCLUSION

The contour maps made for the radiation belts were proven to be accurate, as can be seen by the peak distributions of fluxes both for the proton and electron belts, which resembles the model of Spenvis[5] in Figure 4.

Quantitatively, one can notice the fluxes found through maps in Figures 5 and 6 are about one order of magnitude greater than the ones in Figure 4. That was expected, since the threshold energy chosen for this work was a lot more permissive for both belts: 0.15 MeV instead of 1 MeV for the electrons and 4 MeV instead of 10 MeV for the protons. That takes into account a bigger number of particles in each point of space, since those with energies lower are excluded in Figures 4, but not in the model developed for this paper.

For future perspectives, the first step is to include a dynamic model of the magnetic axis in the algorithm. That includes changing Earth's inclination throughout the year with respect to the Moon's orbit, in order to make the belts suffer an inclination in the moment of the orbital maneuver, as it happens physically. In this way, the trajectories won't cross directly the central part of the radiation belts during most of the trajectory, but will cross its borders, which minimizes the amount of radiation absorbed by the spacecraft by choosing the period of the year in which the inclination is most favorable to a mission, so the fluence of particles can be further optimized.

ACKNOWLEDGMENT

The authors would like to acknowledge their appreciation for the support from the National Council for Scientific and Technological Development (CNPq), through grants #300923/2017-1, #406841/2016-0, #301338/2016-7, #312813/2013-9 and #114190/2018-6; for the support from So Paulo Research Foundation (FAPESP), through grants #2018/16442-6, #2016/24561-0 and #2016/23542-1; and the financial support from the Coordination for the Improvement of Higher Education Personnel (CAPES).

REFERENCES

[1] F. Topputo and C. Zhang, "Survey of direct transcription for low-thrust space trajectory optimization with applications," *Abstract and Applied Analysis*, Vol. 2014, Hindawi, 2014.

[2] W. P. Olson and K. A. Pfitzer, "A Quantitative Model of the Magnetospheric Magnetic Field," *Journal of Geophysical Research*, 1974.

[3] M.-A. Chavy-Macdonald, "Strategies and Geant4 Simulations for Radiation Protection on an EML-2 Mission," 06 2015, 10.13140/RG.2.1.2646.2881.

[4] H. B. Garrett, *Guide To Modeling Earths Trapped Radiation Environment*. American Institute of Aeronautics Astronautics, 1999.

[5] SPENVIS, "Background: Trapped particle radiation models," 2010.

[6] D. Leonard, "C version of NASA's main radiation modelling program," 1998.

[7] A. Sukhanov, G. Barbosa, A. Prado, O. Winter, J. Martins, and E. Macau, "Estimation of the radiation hazard to a spacecraft passing the Van Allen belts in a low thrust transfer," *IAA Conference on Dynamics and Control of Space Systems, 3 (DYCOSS)*, 2017.